Humin based by-products from bioprocessing as potential carbonaceous source for synthesis gas production

Journal:	*Green Chemistry*
Manuscript ID:	GC-ART-07-2014-001324.R2
Article Type:	Paper
Date Submitted by the Author:	17-Sep-2014
Complete List of Authors:	Hoang, Thi Minh Chau; University of Twente, Faculty of Science and Technology van Eck, Ernst; Radboud University Nijmegen, Institute for Molecules and Materials Bula, Wojciech; University of Tokyo, DBGS Gardeniers, (Han) J G E; MESA+ Institute for Nanotechnology, TNW-MCS Lefferts, Leon; University of Twente, Faculty of Science and Technology Seshan, K; University of Twente, Faculty of Science and Technology

Table of content entry

Humin based by-products from bioprocessing as potential carbonaceous source for synthesis gas production

T. M. C. Hoang, E. R. H. van Eck, W. P. Bula, J. G. E. Gardeniers, L. Lefferts and K. Seshan

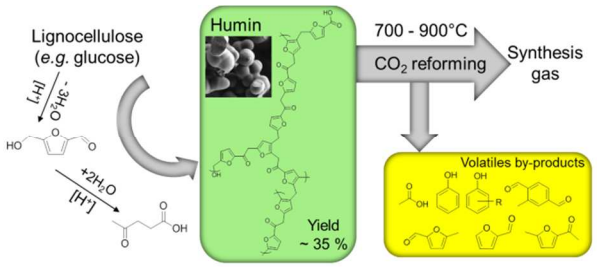

Valorisation of humin by-products: chemical structure of humin and the evolution as well as reactivity of humin in dry reforming

Journal Name

RSCPublishing

ARTICLE

Humin based by-products from biomass processing as potential carbonaceous source for synthesis gas production†

Cite this: DOI: 10.1039/x0xx00000x

Received 00th January 2012,
Accepted 00th January 2012

DOI: 10.1039/x0xx00000x

www.rsc.org/

T. M. C. Hoang,[a] E. R. H. van Eck,[b] W. P. Bula,[c] J. G. E. Gardeniers,[d] L. Lefferts[a] and K. Seshan[a]

Lignocellulosic biomass is addressed as potential sustainable feedstock for green fuels and chemicals. (Hemi)cellulose is the largest constituent of the material. Conversion of these polysaccharides to bio-based platform chemicals is important in green chemical/fuel production and biorefinery. Hydroxymethyl furfural, furfural and levulinic acid are substantial building blocks from (poly)saccharides. Synthesis of these molecules involves acid catalysed hydrolysis/dehydration reactions which leads large formation of insoluble by-products, called humins. Humin obtained from dehydration of glucose is used in this study. Fractionisation of humin was investigated using various solvents (*e.g.*, Acetone, H_2O, and NaOH 1%). Characterisation of humin using various techniques including ATR-IR, HR-SEM, solid state NMR, elemental analysis, Raman spectroscopy and pyrolysis *etc.* confirms its furan rich structure with aliphatic oxygenate linkages. Influence of thermal treatment on humin was investigated. Humin undergoes a lot of changes both in morphology and structure. Humin loses *ca.* 45 wt.% when preheated to 700 °C (prior the gasification temperature) and contains above 92 wt.% C in mainly aromatic/graphitic structures. Valorisation of humin via dry reforming was studied. Non-catalytic dry reforming of humin is very difficult, however, alkali catalyst (*e.g.*, Na_2CO_3) can enhance reaction rate tremendously.

1. Introduction,

Lignocellulosic biomass with its abundance and availability is addressed as a potential and sustainable feedstock for green fuels and chemicals[1-3]. (Hemi)celluloses, comprising 70-80 wt.%, are the largest constituents of lignocellulose[4]. Hence, conversion of these (hemi)celluloses, consisting of carbohydrate units, is crucial in the bio-refinery[5, 6]. In 2004, the US Department of Energy (DOE) published a report of top value added chemicals from carbohydrates. The embraced platform chemicals were selected based on factors, such as, available existing technology, and versatility of the compound to serve as a building block for production of wider derivatives with potential markets[7]. Later in 2010, a revised version of this guideline (The "Top 10 + 4") was published which added more criteria, taking into account extensive newer literature, multiple product applicability, possibility of direct substitution, scope for industrial scale-up etc[8]. Hydroxymethyl furfural (HMF), furfural (FF) and levulinic acid (LA) are among this top list of bio-based primary building blocks[7, 8]. These products are typically made by dehydration of sugars derived from carbohydrates. Even though the preparation of HMF or LA *via* dehydration of fructose was already reported in 1970's[9-12], research on this topic has drawn intensive interest after the DOE's report and especially the potential to produce transportation fuels from carbohydrates as stated in a paper in Science by Dumesic *et al.*[13]. The pathways to convert lignocellulosic biomass to the above platform chemicals

[a] *Catalytic Processes and Materials, Faculty of Science & Technology, MESA+ Institute for Nanotechnology, University of Twente, 7500 AE Enschede, The Netherlands, Phone: +31 (0) 53 489 3033; E-mail: k.seshan@utwente.nl*
[b] *Physical Chemistry/Solid-State NMR, Institute for Molecules and Materials, Radboud University Nijmegen, P.O. Box 9010, 6500 GL Nijmegen, The Netherlands.*
[c] *Department of Bioengineering, Graduate School of Engineering , The University of Tokyo, KBIC 212, 7-7 Shin-Kawasaki, Saiwai-ku, Kawasaki, 212-0032, Japan*
[d] *Mesoscale Chemical Systems, Faculty of Science & Technology, MESA+ Institute for Nanotechnology, University of Twente*

† Electronic Supplementary Information (ESI) available: See DOI: 10.1039/b000000x/

include separation of poly-saccharides from biomass, hydrolysis of the polysaccharides to oligomer/mono carbohydrates (sugars) and dehydration of sugars. Both hydrolysis and dehydration reactions are conventionally performed in aqueous phase using acid catalysts[4, 14]. One of the major problems of these acid catalysed aqueous processes is the formation of large amounts of soluble and insoluble polymeric side-products, generally called as soluble humin and humin, respectively. The latter is sometimes also called humin-like substance, char or coke.

Table 1 summarises recent studies on HMF/FF/LA/γ-valerolactone (GVL) synthesis from carbohydrates. As can be seen, the selectivity to humin depends on substrates used, catalysts, reaction medium, temperature *etc*. When the reaction is carried out in aqueous phase, the selectivity to humin can be as high as above 50% on carbon basis. The formation of humin is more severe with glucose than fructose. Unfortunately, glucose is the most abundant monosaccharide present in lignocellulose; in fact D-glucose is the only monomer of cellulose. Much attention effort has been made to supress the formation of humin (see Table 1). Most used options include performing the dehydration in: (i) organic solvent (*e.g.*, DMSO), (ii) ionic liquid or (iii) biphasic system (aqueous/organic solvent). Another option is combining the dehydration with esterification/etherification. The biphasic system employs, beside water, organic solvents such as toluene, benzene, IBMK, THF. They extract HMF/FF rapidly from the aqueous phase, minimising the condensation reaction between sugar substrate and HMF/FF. In the esterification/ etherification approach, LA/HMF interacts with an alcohol (*e.g.*, methanol, ethanol; alcohol/water varies 4.5 - 10) forming ester or ether, respectively, thus blocking the reactive functionalities in order to avoid further condensation reactions. Although use of an organic solvent or ionic liquid improves the selectivity to HMF or LA substantially, separation of the products from the reaction medium remains challenge. In addition, low concentration of the products formed (LA, HMF) and their higher boiling points compared to solvent (alcohol) makes separation/purification energy intensive and expensive.

Recently, Alonso *et al.*[15] proposed a green, conceptual process using alkyl-phenol, derived from lignin, as the organic solvent. The advantage includes its higher boiling point and stability in the sulphuric acid reaction medium. Further, alkyl-phenol is also suitable as medium for the hydrogenation of LA to GVL – a bio-based fuel. Therefore, the synthesis of HMF/LA *via* homogeneous acid catalysed aqueous route is still of interest. However, conceptual design of both the Biofine process (a commercial pilot plant, reference[16], Table 1) and the process proposed by Alonso *et al* produce 25-45 wt.% of humin. Valorisation of this by-product is therefore crucial for making the whole biomass conversion economical and environmentally viable.

Although humin as a by-product is known for a long time, its use as feedstock is limited to combustion. Further, its chemical structure and properties is not well understood. Generally, it is suggested that humin is a heterogeneous polymeric by-product from carbohydrate conversion which result from the condensation reactions between the carbohydrate (*e.g.*, glucose, fructose) and its intermediates formed during transformation to HMF/FF/LA. Since humin contains *ca.* 60 wt.% C[17-19], it can be used as feedstock for production of synthesis gas or hydrogen *via* gasification. Hydrogen is ubiquitous in biorefinery[20], *e.g.*, conversion of LA to GVL, hydrogenation of glucose to sorbitol. However, minimization of the use of external H_2 for making biofuels/green chemicals is mandatory[20]. From this point of view, efficient conversion of humin to H_2 or syngas ($CO+H_2$) is extremely interesting. Producing H_2/syngas from humin which is considered as waste residue would allow complete use of feedstock carbon in the sugar conversion processes, enhancing the environmental factor of the end targeted product.

In our previous paper, sustainable H_2 from humin was demonstrated *via* catalytic steam reforming route[21]. We had briefly discussed the nature of humin residue at elevated temperatures required for reforming reaction. Humin at this state mainly consists of aromatic/graphitised carbon structure. Additionally, during heating humin to reforming temperatures, part of carbon content was lost as volatile organic components (*e.g.*, up to 25%). Thermal steam reforming of humin is difficult, however, complete conversion of humin could be achieved using an alkali based catalysts (*e.g.*, Na_2CO_3). Loss of catalyst occurs during steam reforming due to formation of volatile sodium species (*e.g.*, Na, Na_2O_2)[21, 22]. Adding small amounts of CO_2 to the reactive feed gas improved the stability of the catalyst by maintaining sodium in the carbonate form. This implies that the actual gasification process can be combination of steam reforming and CO_2 (or dry) reforming. Therefore, understanding the properties and nature of humin residue during the treatment and reforming in CO_2 is necessary.

In this paper, we investigate the characteristics of humin, derived from D-glucose, and used it as a model feedstock for gasification. This includes compositional, structural, morphologic details of the humin residue heated to various temperatures as required for gasification. Kinetics of non-catalytic dry reforming of humin as well as the influence of sodium carbonate to the gasification rate is elucidated. These results not only give a thorough understanding of humin, an abundant waste in biorefinery, but also reveal the real nature of the feedstock for gasification. In addition, this information would be beneficial for consideration of the catalysts to be used for the complete gasification process as well as implementation of various stages for designing the process plant.

2. Experimental

All chemicals used in this study were analytical grade, purchased from Sigma-Aldrich and used without further purification.

Table 1. Summary of recent research on synthesis of HMF/FF/LA from (poly)saccharides

Sugar substrate	Catalyst	Medium	Time (h)	T (°C); P (MPa)	Humin Yield (*)	Selectivity (**)	Author group
D-Fructose	HCl 0.25-1M	H_2O	10	95	16-34	80-64	Kuster *et al.*.[9]
HMF	HCl 0.5-2M	H_2O	9	95	8-18 wt.%	70-84	
D-Glucose	Fe - pillar montmorillonite	H_2O	24	150-170	8.75-11.25	13 (LA entrapped in humin)	Lourvanij, K. Rorrer, G. L.[23]

Kraft paper pulping	$[H^+]$ 1-5 wt.%	H_2O	0.5	195-230	30-40	60-70	Fitzpatrick, S.W - Biofine[16]
D-xylose	MCM-41-SO_3Hs, MCM-41-SO_3Hc, hybrid SO_3H	H_2O	24	140		47 -50 (furfural)	Dias, A. *et al.*.[24]
	MCM-41-SO_3Hs, MCM-41-SO3Hc, hybrid SO_3H	DMSO	24			61-82	
	MCM-41-SO_3Hs, MCM-41-SO_3Hc	IBMK/ H_2O	24			59-61	
	MCM-41-SO_3Hs, MCM-41-SO_3Hc	Toluene/ H_2O	24			83-96	
D-xylose	MCM-41-type niobium silicates	Toluene/ H_2O	6	140-160		20-45	Dias, A. *et al.*.[25]
D-xylose	MP15CsPW, MP34CsPW, LP15CsPW	DMSO	8	140		17-49	Dias, A. *et al.*[26]
D-xylose	MP34PW	Toluene/ H_2O	8	160		45-60	Dias, A. *et al.*[27]
HMF	H_2SO_4 0.05 – 1M	H_2O	2	140-180		60-90	Girisuta, B *et al.*[18]
D-Glucose	H_2SO_4 0.05 – 1M	H_2O	2	140-200		40-60	Girisuta, B *et al.*[28]
Cellulose	H_2SO_4	H_2O	2	150	40	60	Girisuta, B *et al.*[29]
HMF		H_2O	0.8	350; 25	21		Chuntanapum, A. & Matsumura, Y.[30]
D-Glucose	TFA 0.1 – 1M	H_2O	1	180	large amount	57	Heeres, Hans *et al.*[31]
Fructose	FA/TFA + Ru/C	H_2O	8	180	34	66 (LA+GVL)	
D-Glucose	H_2SO_4/HCl	BMIMCl	3	120	16	84	Chidambaram, M. & Bell, A. T.[32]
	CF_3SO_3H				21	79	
	solid acid				7-14		
Fructose	NaCl+$B(OH)_3$	Biphasic	0.75	150		60-65	Hansen, T. S. *et al.*[33]
Levoglucosan	Amberlyst 70	H_2O	3	170	43 wt.%		Hu, X. & Li, C. Z.[34]
		MeOH/H_2O = 10		170	5	95	
		MeOH/ H_2O = 1		170	22	*ca.* 50	
D-Glucose	Amberlyst 70	MeOH/ H_2O = 10	3	170	ca. 3%		Hu, X. *et al.*[35]
		MeOH/ H_2O =0.22		170	23		
Xylose	$Yb(OTf)_3$	H_2O	~1.5	88	96.49 (27.5)	1.75 (0.5)	Weingarten, R. *et al.*.[36]
Furfural	$Yb(OTf)_3$			88	10		
Xylose	Zr-P			160		50	
Fructose	HI+Ru/Pa-cat	Benzene/ H_2O =0.4	2	75-90		60-70	Yang, W. & Sen, A.[37]
	HI+Ru/Cl_3	H_2O		90	significant	15.6	
Hexose	$LnCl_3$ (Ln = Sc, Y, La) in N,N-dimethyl-acetamide (DMA)	H_2O	3		>50%		Beckerle, K. & Okuda, J.[38]
Xylose	5% Amberlyst 70	MeOH / H_2O = 4.5	3	170	12 - 57 wt%		Hu, X. *et al.*[39]
		MeOH/ H_2O = 10-0.22	3	150	4 - 16 wt%		
D-Glucose	HCl	H_2O	2.5	160-200	31.6	*ca.* 48-56	Weingarten, R. *et al.* [40]
Cellulose	Amberlyst 70	H_2O	2.5	150-180	49.6 (+5.5)	*ca.* 44.9	Weingarten, R. *et al.* [41]
D-Glucose	$AlCl_3$	EtOH/ H_2O =9	0.5	160		77	Yang, Y. *et al.*[42]
D-Fructose				160		72	
Glucose	0.05 g Sn-β; 0.05 g Amberlyst-70	H_2O / biphasic=0.1	0.66	130		*ca.* 58-65	Gallo, J. M. R. *et al.* [43]
Fructose, Glucose, Sucrose, β-cyclodextrins	13% Amberlyst 70	EtOH/water=0.5	3	175	14-16	60-74	Hu, X. *et al.*[44]
Levoglucosan, Maltose, Raffinose					*ca.* 18	47-65	
Galactose					23	45	
Glucose	ZrPO	H_2O	6.5		50	33	Ordomsky, V. V. *et al.*[45]
	NbPO	Biphasic	9			*ca.* 65	
Cellulose	$NaHSO_4$+$ZnSO_4$	THF/ H_2O =10	1.5	140-180	40-7	37-70	Shi, N. *et al.*[19]

(*) Humin yield is estimated as C yield when not specified.
(**) Selectivity for all useful products when not specified and based on C balance

2.1 Humin preparation and purification

Humin was prepared as following. A mixture of 500 ml glucose 1 M and sulphuric acid 0.01 M were placed in quartz insert of 1 L Büchi stirred autoclave. The mixture was flushed with helium at room temperature to remove air. It was then heated to 180 °C and kept at that temperature for 6 h with stirring rate of 500 rpm. After that the reactor was cooled down to room temperature (RT). Insoluble products were filtered on a Brüchner funnel and washed with 3 L of de-mi water. The solid humin was then dried at 80 °C for 24 h and subsequently ground to granular powder (< 300 μm). Humin after this step was denoted as HG1. The yield of HG1 in comparison with the sugar feedstock is 35 ± 1 wt.%. In order to remove the sugar derivatives entrapped in humin, HG1 was then purified using Soxhlet extraction with water for 24 h. After that, the solid was dried in vacuum oven at 80 °C for 24 h and denoted as HG2.

Solubility of humin in various solvents (*e.g.*, water, acetone *etc.*) was determined using standard analytical methods applied for wood and pulp approved by Technical Association of the Pulp and Paper Industry (TAPPI). Water solubility of humin was performed and estimated using "TAPPI T207 cm-99 Standard". Acetone extractives of humin were carried out according to "TAPPI T204 cm-97 Standard". One per cent sodium hydroxide solubility of humin was determined using "TAPPI T212 om-02 Standard". Residues of humin after the extraction in hot water, acetone and NaOH 1% are denoted as HG1-W, HG1-Ac, and HG1-NaOH 1 %, respectively. HG1-W was further extracted in acetone and tetra hydro furan (THF) using method described in the "TAPPI T204 cm 97". Short description of these methods can be found in the Supplementary Information. The solvents containing extractives were later analysed by LDI-TOF and ESI mass spectrometric techniques.

For industrial gasification, it is required to use as-prepared humin with minimal washing and purification to reduce cost and energy. Therefore, in order to establish the characteristics of humin under dry reforming conditions (*viz.* heating in CO_2 rich atmosphere) HG1 was used and preheated under 100 ml/min flow of 40 vol.% CO_2/N_2. Furnace temperature was increased at the rate 10 °C/min, kept constant at the desired temperatures (*e.g.*, 400, 500, 600 and 700 °C) for 12 minute, and then cooled down to room temperature.

2.2 Characterisation

Elemental composition was determined with a Perkin-Elmer elemental analyser (Thermo Scientific Flash 2000). The analyser was equipped with a two-reactive-bed-column and calibrated with acetanilide. Carbon, hydrogen and nitrogen were estimated based on the amount of water, CO_2 and N_2 from the chromatogram. Oxygen content was calculated as the remaining part.

Morphology of humins was analysed by High Resolution Scanning Electron Microscopy (HR-SEM) using HR-SEM Zeiss 1550.

Specific area was determined from t-plot in BET method with a Micromeritics Tristar instrument. Humin samples pre-heated at various temperatures (300 - 700 °C) and fresh humin were degassed at 300 °C and 150 °C, respectively for 24 h prior to the analysis.

For ATR-IR analysis, solid humin (HG1) and its acetone soluble fraction were placed or deposited directly on a ZnSe crystal. The crystal with samples was dried in vacuum oven for 30 minute at 50 °C to remove the solvent and minimise the moisture between humin particles. This analysis was acquired with a Bruker Tensor 27 infrared spectrometer equipped with a MCT detector. All ATR-IR spectra were recorded at *ca.* 21 °C by averaging of 128 scans with resolution of 4 cm^{-1}.

Qualitative analysis of components in the effluents after extraction in water and NaOH was performed with a mass spectrometry detector (MSD) (SL/G1956B, Agilent) equipped with an electro-spray ionization (ESI) liquid-phase interface (G1948A, Agilent). The effluents were sent to the ESI chamber by a syringe pump with flow-rate 0.5 ml/min. ESI was operated in positive mode with fragmentation voltage of 200 V, drying gas temperature 350 °C.

Extractives of humin in acetone were dissolved in THF (0.1 g/ 10 ml THF) for gel permeation chromatography (GPC) analysis. The GPC data was obtained using a GPC system of Agilent Technologies 1200 series equipped with a reflective index detector, calibrated with polystyrene standards (molecular masses between 162 and 29510 Dalton).

For Laser Desorption Ionisation Time of Flight MS (LDI TOF MS), humin was dispersed in water using ultra-sonication bath. 2 μl of the mixture was pipetted onto the stainless steel MS plate. The mass spectra were recorded using a Waters SYNAPT HDMS MALDI-TOF mass spectrometer operated in positive ion mode. Poly-ethylene glycol standards were used for calibration.

Carbon structure of humin residues was identified by Bruker Senterra Raman spectrometer with laser wavelength 532 cm^{-1}. Humin particles are black bodies and can be heated up easily under the laser beam, which can cause structural influence or damage to the material. To diminish this thermal emission, samples were mixed with spectroscopic grade KBr and ground with mortar and pestle. The powder mixtures of 0.5 wt.% humin in KBr were then pelleted. Laser power of 10 mW, contact time 1 s was used. Each Raman spectrum represents the average of 50 scans with spectral resolution of 4 cm^{-1}.

Solid state ^{13}C Nuclear Magnetic Resonance spectra of humin were acquired on a 14.1T Varian VNMRS system at Magic Angle Spinning (MAS) frequency of 20 kHz using 3.2 mm MAS probe. Contact time 1000 μs and 50 μs were used for cross polarization (CP) and single pulse (SP) experiments, respectively. The spectra were referenced to adamantane.

The setup and procedure for pyrolysis experiments was described elsewhere[46]. CO_2/Ar mixture (CO_2 40 vol.%, total flowrate of 70 ml/min) was used to mimic the dry reforming experiment. For the experiment to identify volatiles as function of temperature, the furnace was heated from RT to 400 °C in less than a minute, kept at that temperature for 15 minutes before it was raised to the next temperature (*e.g.*, 500, 600, and 700 °C). Condensable products were collected during each step. In a separate experiment one sample was heated directly to 700 °C (heating rate *ca.* 925 °C/min). The condensable products formed during this experiment were diluted with acetone and analysed by an Agilent 7890AGC coupled with 5975C Mass Spec. The identification was based on NIST (National Institute of Standards) 2008 library.

2.3 Thermo gravimetric analysis and gasification experiments

Standard TG analyses as well as the gasification experiments were performed in a Mettler Toledo thermo gravimetric analyser (TGA/SDTA/ 851e). Solids gasification experiments are difficult to carry out in laboratory scale and TG provide one easier way to study such reactions. Gas supply to

the TGA chamber included two streams: reactive gas stream containing mixture of CO_2 and Ar (flowrate of 80 ml/min) flowing in adjacent to the top of the crucible and protective gas stream using Ar (20 ml/min) which was blown horizontally from a side of the chamber. The average concentration of CO_2 fed to the TGA chamber was varied from 5 to 40 vol.%. A mass spectrometer (Balzer QMS 200F) was connected to the outlet valve of the chamber to monitor the gas evolution during these experiments. Humin samples with initial weight of 2 – 3 mg were placed in an alpha alumina crucible (volume of 70 µl) and dried *in situ* at 105 °C for an hour before the furnace was raised to the desired temperatures (750 – 900 °C) and kept there for 60 – 300 minutes. After that the furnace was cooled to room temperature. Heating or cooling rate of 10 °C/min was used. It should be noted that the conversion rate was independent of sample mass below 5 mg; therefore, there was no mass transfer limitation from gas to solid humin.

In the case of catalytic dry reforming, purified humin (HG2) and various amounts of Na_2CO_3 (Humin/HG2 mass ratio ~ 0.5 – 2.5/100) were mixed together using a Fluxana mixer (MU-K-Mixer_50 Hz) for ~ 20 minutes which mainly mixes the powders by shaking, albeit in the presence of two small plastic balls. In these catalytic experiments for determining the activation energy, humin (HG1) and Na_2CO_3 were ball-milled together for 20 minutes with frequency of 20 Hz.

All conversion values used in this study are cumulative and calculated as following:

$$\text{Conversion } (X_i) = \frac{m_0 - m_i}{m_0 - m_{salt}} \quad \text{(w/w)}$$

$$\text{Residue weight} = 1 - X_i \quad \text{(w/w)}$$

$$\text{Gasification rate} = \frac{\partial X_i}{\partial t}\left(\text{min}^{-1}\right)$$

Where: m_0, m_i m_{salt} are mass of humin after *in situ* drying at 105 °C for 60 minutes and at the interest point and mass of Na_2CO_3 in the initial mixture, respectively; X_i is conversion at the interest point.

3. Results and discussion

3.1 Characteristics of pristine humin (HG1)

It can be seen from Table 1 that the dehydration of sugars can be achieved in a wide range of experimental conditions, *viz*, temperature, retention time and with diverse sugar feedstock. We chose, humin from glucose dehydration as the representative humin for this study. This is because glucose conversion is one of the most studied routes for making HMF due to its commercial significance. In spite of the choice of the sample, such studies will help establish a basic understanding of the requirements for (catalytic)gasification of humins in general.

HR-SEM images of the pristine humin sample used in this study are shown in **Figure 1- A, B**. It can be observed from Figure 1-A that humin comprises of solid, sphere-shaped agglomerates with wide size distribution (1 – 20 µm). This size range is wider than that reported by Girisuta *et al.* and Van Zanvoort *et al.* [18, 47] (5-10 µm) for humins obtained from HMF, glucose or cellulose using H_2SO_4 as catalyst. According to Van Zanvoort *et al.* reaction parameters such as retention time, agitation speed had strong influence on the morphology of humin. Therefore, the large particle size distribution of humin here can be due to this reason. In our sample, particles below 3 µm have a more defined spherical shape while the larger ones look like smaller spheres aggregated together. The cross section image (not shown) of these particles indicates no clear boundary or interface between the smaller spheres. At higher magnification (**Figure-1B**) smooth surface and a dense core structure of the humin particles can be seen. This is confirmed by BET analysis; the specific area of this pristine humin is negligible.

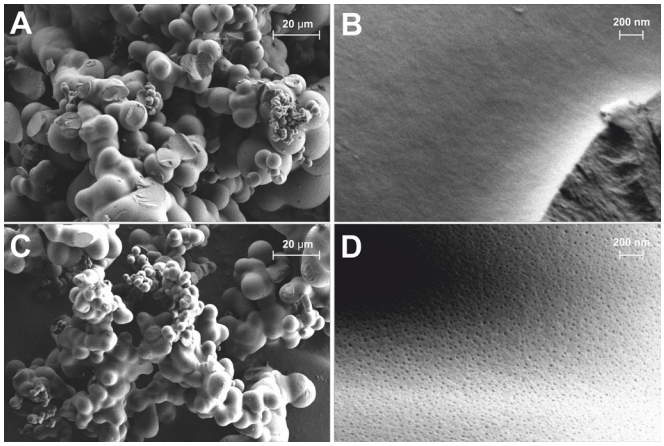

Figure 1. HR-SEM images of HG1 (A,B) and HG2 (C,D) . B, D-SEM images of surface of HG1 and HG2 respectively

Generally, it is suggested that humin is formed by condensation of intermediates formed during dehydration of sugar. Besides, all components which are part of the reaction sequence can also be embedded in the humin matrix. For example Baccile[48] reported *ca.*15 wt.% carbon exists in the form of levulinic acid entrapped in the hydrothermal carbon spheres prepared using a method similar to that for making humin, except that the acid catalyst for de-hydration was generated *in situ*. Hence, it should be possible to extract these embedded components using solvents such as water or acetone. It is observed that extraction solvents changed to brown colour after refluxing with humin. **Table 2** shows the fraction that is extractable and the elemental composition of the residue after extraction. Only 7.5 wt.% of humin dissolves in hot water (~95 °C). Acetone or the solution NaOH 1 wt.% is more effective. While water can extract hydrophilic, light, water soluble components such as HMF, LA; acetone might be capable of removing more polymerised oligomers which can be more

Table 2: Elemental composition of humin and humin fractions

Sample	C	H	O	Dissolved Fraction
HG1	66.3 ± 1	4.4	29.3	0
HG1-W	66.3	4.2	29.5	~7.5 wt.%
HG2	66.1	4.4	29.5	n.a.
HG1-Ac	67.9	4.3	27.8	~11 wt.%
HG1-NaOH 1%	66.3	4.2	29.0	~15.8 wt.%
HG1-W-Ac	65.7	4.2	30.1	n.a.
HG1-W-Ac-F	67.9	4.8	27.2	n.a.
Acetone soluble	63.2	5.4	31.4	

HG1-W-Ac: humin residue after extractions in water then in acetone, HG1-W-Ac-F: is residue of Soxhlet extraction of HG1-W-Ac in THF; n.a - not available

hydrophobic. NaOH can also affect the hydrolysis of oligomers or humin. GC-MS analysis of the solution after Soxhlet extraction of pristine humin (HG1) in acetone confirmed the presence of LA, HMF, 5-methyl furfural, furfural, 2-acetyl furan which are formed during the dehydration of glucose[12]. These identified compounds comprise *ca.* 90 % peak area in the gas chromatogram (not shown). However, it should be noted that the GC-MS can only analyse the more volatile fraction of the extraction solution (boiling point below 250 ˚C). After Soxhlet extraction (24 h for water and 8 h for acetone), the solvent in contact with solid humin became colourless and did not contain any extractable as seen by GC-MS. Thus, it can be assumed that the extraction was complete and able to remove all the embedded components. HR-SEM images of humin after Soxhlet extraction for 24 h in water is shown in **Figure 1-C, D**. There is no clear indication of change in particle size (**Fig. 1-C**). However shallow pores on the surface of humin after the extraction can be seen (**Fig 1-D**). This might be the result of removal of the oligomers or precursors of humin. This is in agreement with the growth mechanism of humin or carbon spheres proposed by Yao *et al.*[49] for glucose, where the spheres grow by condensation at the external surface also implying presence of oligomers at the external surface.

Table 2 also shows the elemental composition of humin and its residues after purification. In addition to C, H, O contents, small amounts of sulphur (0 – *ca.* 1000 ppm) were also found in some batches of humin. This S content can result from the sulfonation reaction between sulphuric acid and humin or sugar substrates during the dehydration. The elemental composition of pristine humin in this research is similar to those reported by others[18, 47, 50]. Variations in the carbon content of humin samples are the result of different extent of dehydration and depend on experimental conditions[17]. Within our experiments, only very minor changes in elemental composition were observed **(Table 2)** for humin and its residues after various extraction steps in different solvents. The fraction extracted with acetone still contains low mass sugar intermediates such as HMF and LA.

GPC analysis of the acetone soluble fraction provide a number-average-molecular mass of 302 Dalton and 90 % of the sample eluting from the GPC column has mass below 2000 Dalton (S1, Supplementary Information). Lower masses include (i) 110 Dalton which can be acetyl furan or methyl furfural, (ii) 138 Dalton corresponding to the formula $C_7H_6O_3$, and (iii) 252 Dalton corresponding to acetal of 2-HMF. The higher masses might be from the oligomer by-products in the de-hydration of glucose or humin segments which can be dissolved in acetone or the recombination/condensation of the low mass molecules (HMF, LA, FF, 2-acetyl furan *etc.*). The higher mass molecules can be considered as humin precursor/fragments. MS analysis of soluble humin in NaOH 1%, water (by ESI-MS, figure S3) as well as solid humin (LDI-TOF MS, figure S4) shows a significant peak of 301 Dalton. In addition, set of peaks with 300 Dalton difference were observed in MS spectra (**S2-4**, Supplementary Information). From the relative ratio of the peaks 301+1 and 301 Dalton, the number of carbon in the molecule is estimated as 17. Regarding the elemental composition, the mass 301 can be assigned to the chemical formula of $C_{17}H_{16}O_5$. All resolved masses from MS analysis are below 3000 Dalton.

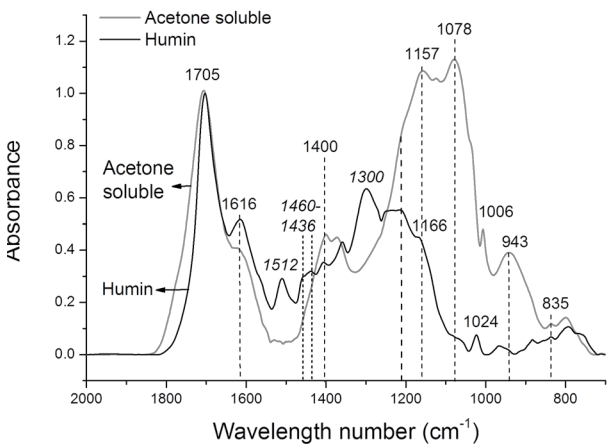

Figure 2. ATR-IR of HG1and its acetone soluble fraction

Comparison of the ATR-IR spectra of pristine humin and the fraction that is soluble in acetone is presented in **Figure 2**. Peaks at 1705 cm^{-1}, corresponding to C=O asymmetric stretching typical for carbonyls, and 1616, 1400 cm^{-1} to 2-substituted furans, are as expected present in samples. Peak at 1512 cm^{-1}, typically corresponds to poly-substituted furans and since it is present only in humin sample, it may be due to furan structure present in the framework. The peaks at 1436 and 1460 cm^{-1} can be assigned to CH_2 deformation vibrations in aliphatic chains. The shift of peak at 1460 to lower range (*i.e.*, 1436 cm^{-1}) is due to being adjacent to double bonds or carbonyl groups. 1024 and 1300 cm^{-1} in humin corresponds to C=C stretching and C-H rocking, respectively, in olefinic groups. Strong peaks at 1078 and 1157 cm^{-1} corresponding to C-O stretching in alcohols is seen in the extracted sample.[51]

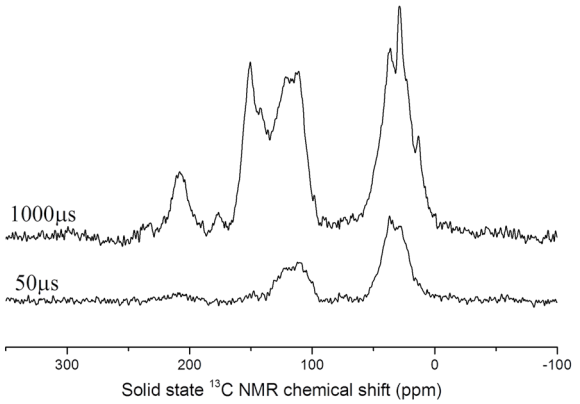

Figure 3. Solid state ^{13}C-NMR of pristine humin (HG1) with long contact time (CP mode) and short contact time (SP mode)

Figure 3 shows ^{13}C - solid state NMR spectra of humin recorded at long contact time (1000 µs) using cross polarization mode and short contact time (50 µs) with single pulse mode. The spectrum from short contact time analysis shows functional groups which contain proton (H). By comparing spectra between these two NMR modes, it's possible to identify the functional groups which have the same value of chemical shift (*e.g.*, ketone *vs.* aldehyde or carboxylic acid *vs.* ester). Therefore, the band 210 ppm corresponds to carbon in carboxylic and not in ester group, while 178 ppm represents ketone and not aldehyde[48]. The band from 0 – 50 ppm is assigned to aliphatic groups (CH_x). The main band between 100 and 150 corresponds to sp^2 carbon. According to Baccile *et al.*[48] and Falco *et al.*[52], bands in this region comprises three types of functional groups: (i) furanic carbon at alpha position (150 ppm), (ii) furanic C at beta position (110 ppm) and (iii) sp^2 hybridised aromatic carbon (127 ppm). It can thus be concluded

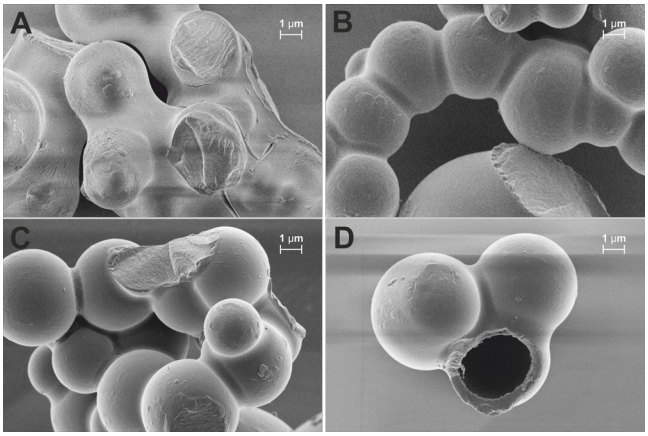

Figure 4. HR-SEM of HG1 preheated in CO_2 at various temperatures: A- 400°C, B – 500°C, C- 600°C, D- 700°C

that humin framework mainly consists of furanic segments with aliphatic linkages decorated by carboxylic and ketone groups.

3.2 Changes to humin during heating prior to gasification

Gasification of humin requires high temperatures, typically 700 - 900 °C. Since humin is made up of an organic matrix that is unstable during heating, it can be expected to undergo changes and the residue that is gasified can be different from the pristine sample at room temperature. Therefore, understanding any changes that occur is very important. HR-SEM photographs of humin sample preheated to various temperatures in CO_2 are displayed in **Figure 4**. There is no clear indication of any change in particle size after heat treatment even up to 700 °C. However, changes in morphology and surface texture are observed. The surface of humin at 400 °C appears to be swollen and the boundary between particles shows neck formation. At 500 °C, spherical shaped particles are clearer to see and the dense structure is maintained in agreement with the similar low (below detection limits) surface areas measured by BET. At 600 and 700 °C, sample becomes very porous with specific area of 463 and 447 m^2/g, respectively. This can be the result of loss of part of humin, *e.g.*, escape of molecules trapped in the humin matrix, as discussed earlier. These are discussed in more detail in the following section. The most surprising result is the appearance of hollow structures

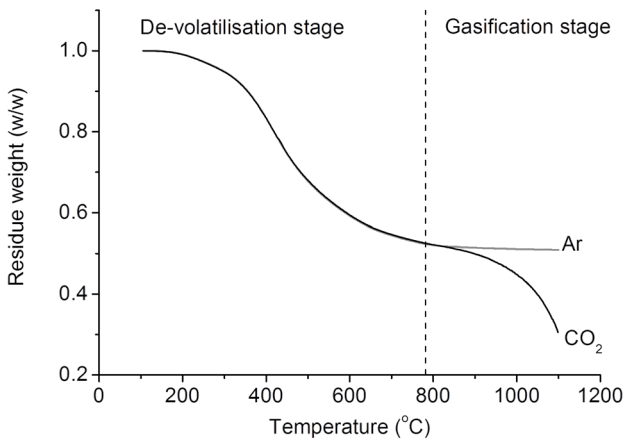

Figure 5. TGA analysis of HG1 in inert (Ar) and 40 vol.% CO_2/Ar. Temperature ramp = 10 °C/min, total flowrate 100 ml/min

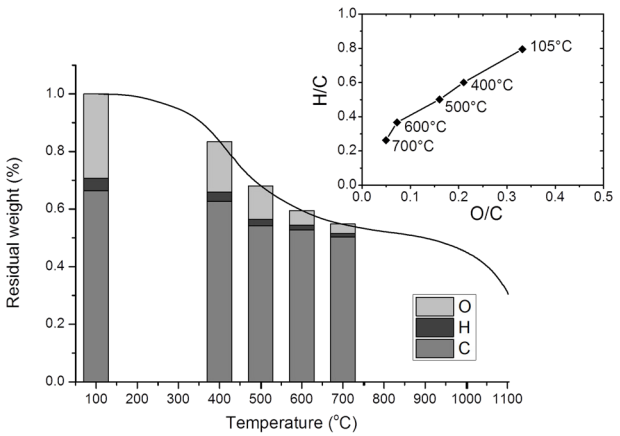

Figure 6. Elemental composition of HG1 residues preheated in CO_2 at 400, 500, 600, 700°C (temperature ramp 10 °C/ min). Inset: Van Krevelen diagram of correspondent humin residues

(**Figure 4-D**) in humin particles at 700 °C. This phenomenon does not occur in the case of heating in inert gas (N_2 – See figure **S5** – Supplementary information). The unique hollow structure could result from faster dry reforming reactions of the materials at the core of humin particles, which is more reactive than those at the shell. This indicates an asymmetric composition across the radius of humin particle. The degree of carbonisation and condensation of the insoluble polymer at the core layer might be lower than that of the shell, which had more contact with acidic medium of the sugar dehydration process. Surprisingly, we did not see this in the case of steam (*ca.* 2 vol.% steam/ N_2)[21]. This probably is because CO_2 is a very mild oxidant and less reactive than steam, in the latter case gasification is possible and occurs everywhere.

HR-SEM analysis visualised the influence of thermal treatment on humin. Other characterisation techniques such as TGA, pyrolysis were employed to gain further insight into the influence of pre-heating on humin. **Figure 5** shows the thermal gravimetric analysis of humin under inert and reactive gas atmospheres. In both CO_2 and Ar, continuous weight loss occurs from 105 °C to 700 °C, followed by a stable period up to *ca.* 800°C. While in Ar the weight loss levels off at a value of *ca.* 45 wt.%, in CO_2 the rate of weight loss increases again above 800 °C and continues rising until 1100 °C. The weight loss below 800 °C can be attributed to thermal de-volatilisation since no clear difference between two curves performed *i.e.*, in reactive gas (CO_2, dry reforming) versus inert Ar. The weight loss in CO_2 atmosphere at higher temperatures results from dry reforming reactions of humin residue. However, even at 1100 °C, final weight loss of only 70 wt.% is achieved implying incomplete conversion and low reactivity of part of the humin residue.

The elemental compositional changes to humin as a function of temperature prior to reaching CO_2 reforming temperature is presented in **Figure 6**. The inset graph illustrates the Van Krevelen diagram of these intermediate humin residuals (the figures indicates pre-treatment temperature of corresponding residues). It reveals continuous de-oxygenation occurring when humin is heated. Loss of oxygen and change in elemental composition is caused by the release of volatile products as well as decomposition of reactive functionalities in its structure to form organic volatiles and gas (*e.g.*, dehydration, decarboxylation, decarbonylation). Humin heated to 700 °C, close to the onset of reforming, contains 92 wt.% carbon. And

the corresponding changes in H/C ratios of the samples indicate more and more aromatisation of humin residue as the result of heating. Similar van Krevelen diagrams were reported for pyrolysis char from pectin[53], and glucose[54].

Online analysis of the gas phase during the TGA experiment showed that the products belong to two groups: (i) permanent gases (*e.g.*, H_2O, CO_2, H_2) and (ii) organic volatiles. The former was monitored by QMS (**Figure 7**) while the organics were monitored in a separate experiment, discussed later. The formation of gas products in both thermal decomposition (**Figure 7-A**) and in CO_2 reforming (**Figure 7-B**) show similar trends. Signal for H_2O has 2 peaks at *ca.* 450 °C and *ca.* 780 °C. The first peak can be attributed to dehydration of sugar derivatives while the second might contribute to dehydration/condensation of phenols or aromatic aldehydes. CO_2 in the exhaust gas as result of decarboxylation of carboxylic groups in humin structure peaks at ca. 390 °C or 396 °C in inert – Ar or in rich CO_2 atmosphere, respectively. The signal of CO reaches to highest point at ca. 410 °C in CO_2 atmosphere. It then levels off from 550 °C till 800°C and rises rapidly above 800 °C. The first peak of CO is due to de-carbonylation of ketone groups in humin while the rise at elevated temperature range corresponds to the dry reforming reactions. Both decarboxylation and de-carbonylation not only lead to decrease of O content but also cause loss of C to gas phase. From Fig 6, it can be seen that most of C loss occurred between 400 and 500 °C. There is no corresponding evolution of CO_x (**Figure 7-A** or **B**) in this temperature range, thus the loss in Fig 6 does not match with the trend of CO and CO_2 evolution in dry reforming atmosphere and might be attributed to other vapour products *e.g.*, organic volatiles. Presence of H_2 is detected in the exhaust stream from the TGA furnace. Dehydrogenation takes place above 600°C and reaches its peaks at *ca.* 750 °C. This might contributes to the sharp slope in Van Krevelen plot between 600 – 700 °C, besides possible aromatisation.

In order to identify the chemical functionalities of the volatile products, fast pyrolysis technique using rapid IR heating was employed[46]. This technique provides an extremely high heating rate, short retention time of the vapour in heated zone therefore, minimising secondary reactions of volatiles. To avoid the influence of sugar derivatives entrapped in the pristine humin (HG1), the humin purified in water for 24 h (HG2) was used for this experiment. The composition of organic volatiles, based on GC-MS area percentage analysis, as function of treatment temperature is illustrated in **Figure 8.** Each bar on the graph represents the composition of the volatiles which release from purified humin – HG2 (no sugar derivatives left in the matrix) throughout each temperature step. The identified volatiles are classified into six groups: furans, cyclopentene-1ones, benzo-furans, phenols, (poly)-aromatics (excluding phenol type compounds), and oxygenate aliphatics.

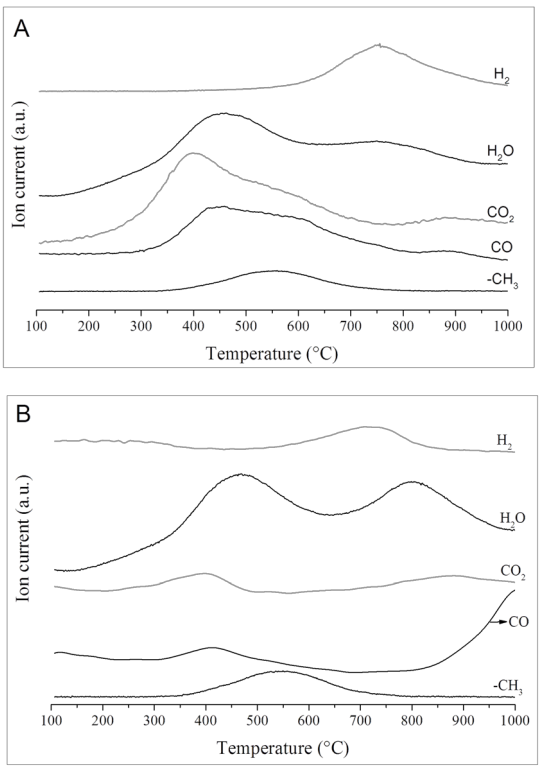

Figure 7. Evolution of gas products followed by Q-MS from heating HG1 under Argon (A) and 40% CO_2 /Ar (B). Ramp = 10 °C/min

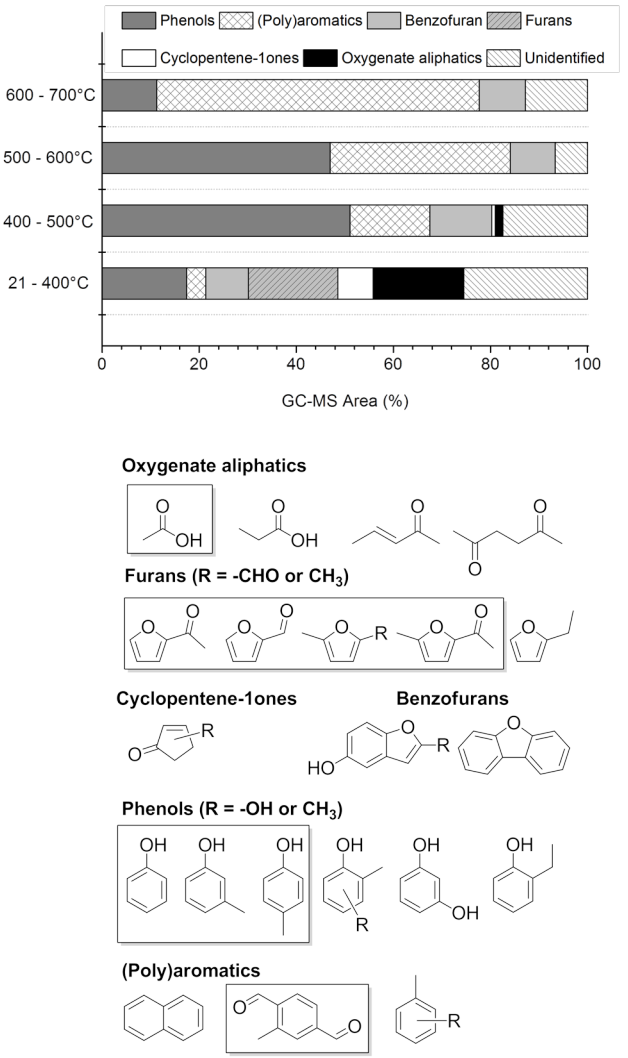

Figure 8. Representative condensable volatiles released during de-volatilisation stage of humin (HG2). Chemical structures in embedded in frame are those identified in 1-step pyrolysis experiment from RT-700°C.

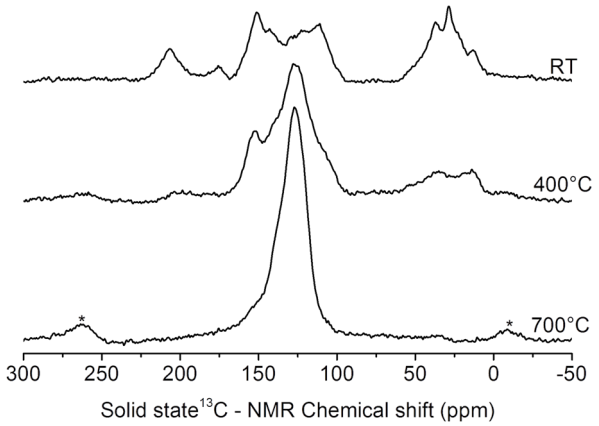

Figure 9. Solid state ^{13}C-NMR of humin (HG1) residues pre-heated at various temperature. (*) is spinning side band

Components of the volatile mixture from 21 – 400 °C are the most diverse with about 60 compounds. Furans, cyclopenten-1ones and some aliphatic oxygenates (*e.g.*, acetic acid, propanoic acid) are present only in this interval. Between 400 and 500 °C only traces of these are observed. Phenols, (poly)aromatics and benzo-furans are the major constituents of volatile stream above 400 °C. The components of volatile mixture not only reflect the chemical structure of humin – furan rich but also reveal the complexity of reaction pathways occurring during heating. In addition, secondary reactions of volatiles might still take place during pyrolysis (heating rate 480 °C.min^{-1}). Accordingly, fewer components were observed when the pyrolysis of humin in CO_2 atmosphere from RT to 700 °C was carried out much more rapidly (heating rate *ca.* 975 °C.min^{-1}).

Solid state ^{13}C NMR can give information about the chemical bonds in humin residues. Figure 9 shows ^{13}C NMR spectra of humin preheated to 400 and 700 °C and spectrum of pristine humin in comparison. Ketone (178 ppm) and carboxylic functional groups (210 ppm) in pristine humin almost disappear in the spectrum of residue at 400 °C. This can be explained by the decarboxylation, decarbonylation to form CO_2, CO (mentioned above) of carboxylic volatiles (*e.g.*, acetic acid, propanoic acid). No presence of these bands is observed in the 700°C-residue. The aliphatic region (0 - 50 ppm) decreases significantly at 400 °C and vanishes at 700 °C. The most important band, 100 – 160 ppm, changes intensively in shape, peak position. Both bands, at 110 ppm and 150 ppm are representative for furan rings decrease extensively while the band at 127 ppm – corresponding to hybridised sp^2 of C=C bond in aromatic ring, increase sharply at 400°C. Sample at 700°C, where the dry reforming initiates, contains one main peak at 127 ppm and a small shoulder at 150 ppm. The one at 127 ppm corresponds to (poly)aromatic, graphitic carbon. The shoulder might be attributed to benzo-furan which was also present in the volatiles released at this temperature interval.

Raman spectroscopy can be used to analyse the structure of carbon. The Raman spectra of humin residue heated from 300 to 700 °C are shown in **Figure 10**. All spectra were normalised to the intensity of the stronger band at 1600 cm^{-1}. It was not possible to record the visual Raman spectrum of pristine humin (HG1) due to increase of photoluminescence background caused by the high H content. Spectra of the pre-heated humin residue consist of two peaks, corresponding to D-band at 1350 cm^{-1} and G-band at *ca.* 1600 cm^{-1}. According to Ferrari and Robertson[55], the D and G band are due to sp^2 C=C. The G band corresponds to the bond stretching of all pairs of sp^2 C in both rings and chains while the D band is due to the breathing mode of sp^2 C in rings. Those, particular spectra of samples above 400 °C are typical for carbonised carbon materials[56]. A clear increase in D band to G band area/height ratio with temperature can easily be observed from **Figure 10**. This means increase in aromatic ring concentration at the higher temperatures[55, 57]. In addition, FHWM of G band peaks is a measure of the crystal order. The decrease of $FHWM_G$ means reducing the disorder in C structure of the residues. The position of G peak (inset of Fig 10) increases with temperature, together with the decrease of $FWHM_G$ and increased I_D/I_G ratio, support the conclusion of transition of humin from amorphous structure to aromatised/graphitised carbon[55].

As mentioned in section 3.1, the molecule mass of 301 Dalton (or masses with 300 Dalton difference) was found in all fractions of humin. Chemical formula of $C_{17}H_{16}O_5$ can be assigned to this mass. Interestingly, the C : H : O atomic ratio of humin is approximately 17:13:5. We believe that this formula is one of the base structural units produced from the hydrolysis depolymerisation of solid humin as well as soluble humin.

From spectroscopic analyses (ATR-IR, NMR), as well as

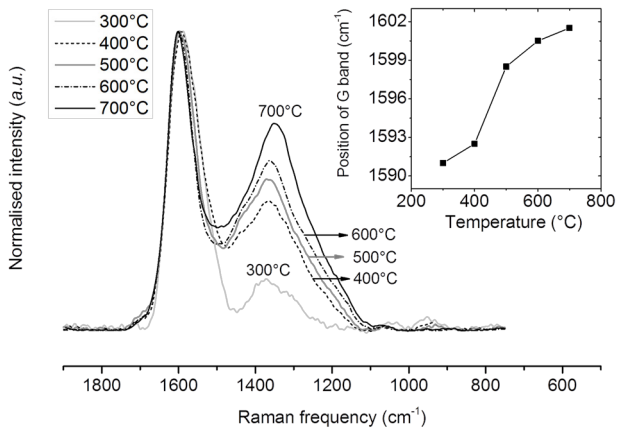

Figure 10. Raman spectra of humin (HG1) residues normalised to G band height. Inset: position of G band peak

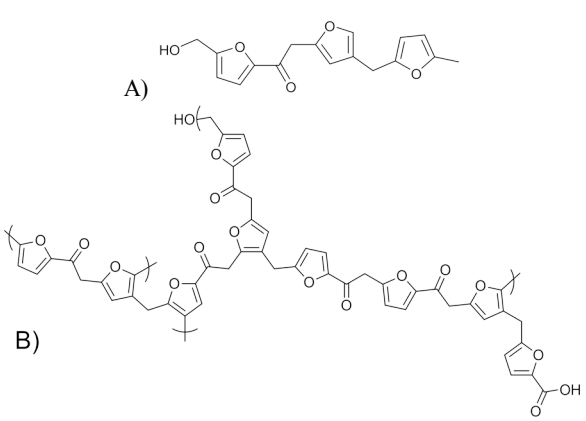

Figure 11. Chemical structure of humin segment with mass of 300 Dalton and proposed model of humin constructed from that segment ($C_{52}H_{40}O_{17}$-from 3 units)

from pyrolysis studies, and taking into account literature information[47, 48] on hydrothermal carbon (which is similar to highly carbonised humin), we propose structure of the formula $C_{17}H_{16}O_5$ as that illustrated in **Figure 11-A**. It is suggested that two furan rings are linked by an acetyl group *via* αC. This is supported by the presence of 2-acetyl furan or 2-acetyl 5 methyl furan in the pyrolysis products of humin. The acetyl linkage is formed *via* de-hydration of two HMF molecules. αC can be linked with βC of other furan ring by CH_2 linkage. Figure 11-B shows the proposed representative structure of humin which is constructed from three proposed units with a carboxylic functional group. It corresponds to the chemical formula of $C_{52}H_{40}O_{17}$. In this report the suggested humin structure is formed *via* a de-hydration pathway of furan type species. It should be noticed that other active components in the medium of de-hydration of sugars such as levulinic acid, formic acid, sugar intermediates can also graft to humin matrix *via* condensation reactions. This model structure shares some common features with the structure of humin from glucose proposed by Van Zandvoort *et al*[47]. However, in our model, acetyl is the major linkage between furan rings due to the consistent presence of acetyl groups in spectroscopic and pyrolysis characterisation analysis. Meanwhile ethyl/ethylene is proposed as major linkage between furan rings in that literature. By various characterisation techniques shown in section 3.2, it is concluded that thermal treatment has very strong influence on humin. Humin undergoes a lot of changes in texture, composition and chemical structure upon heating prior to it reaching gasification temperature. De-oxygenation, de-volatilisation of humin occurs at elevated temperatures. Humin becomes, as a result, more aromatised, graphitised. The actual humin feedstock for gasification contains mainly C (above 90 wt.%) in graphitic/aromatic structure with few oxygen containing groups (*e.g.*, phenolic or benzo-furan). Therefore, the gasification of humin is expected to resemble those of biomass char or coals.

3.3 Non-catalytic dry reforming of humin

Due to the inert, low reactivity of graphitic carbon, thermal reforming of humin would be difficult. Dry reforming reactions of humin residue at elevated temperatures (above 700°C) can be simplified as following:

$$C_{61.3}H_{16}O_3 + 61.3\ CO_2 \rightarrow 122.6\ CO + 5\ H_2 + 3\ H_2O \quad \text{(Eq 1)}$$
$$C_{61.3}H_{16}O_3 + 58.3\ CO_2 \rightarrow 119.6\ CO + 8\ H_2 \quad \text{(Eq 2)}$$

Where $C_{61.3}H_{16}O_3$ is the simplified chemical formula based on the CHO analysis of humin residue preheated to 700°C. Eq 1 illustrates the conversion of [H] and [O] in humin *via* dehydration/dehydrogenation while the [O] in humin is released also in the form of CO in Eq 2. Since humin sample contained about 92 wt.% [C], the major expected product is CO. Selectivity to water and hydrogen would be small during the dry reforming. Conversion during the experiment is estimated from the weight loss during TGA.

Figure 12-A shows the thermal (non-catalytic) dry reforming of purified humin samples (HG2) at various temperatures using the same preheating conditions (10 °C/min). At 750 °C, after 280 minute time on stream, only 7 wt.% is converted. Even at 900 °C, only 20 wt.% of humin is gasified. Compared with lignocellulosic char, reactivity of humin is much lower[58, 59]. This is due to lack of mineral in the humin derived from glucose meanwhile chars from natural lignocellulosic biomass always contains a certain percentage of potassium or other minerals. It is well known that minerals act as catalyst for the reforming reactions. It should be mentioned that HG2 (*viz.* without the contamination of the entrapped sugar derivatives) was used in order to investigate the intrinsic reactivity of pure humin. However, the slope of conversion curve for gasification of pristine humin (HG1) at 900 °C – the dash line in **Figure 12-A** is almost similar with that of purified humin (HG2). This implies those two residues have similar reactivity towards the dry reforming reactions. The impact of the char formed from the sugar derivatives in HG1 during the de-volatilisation stage is minor due to two possibilities: (i) low amounts or (ii) its reactivity falls in the same range of purified humin.

Apparent kinetic orders of the reforming reaction were investigated and the result is shown in **Figure 12-B**. The dry reforming of humin is performed at atmospheric condition. Therefore, CO_2 concentration of 5, 22.5, and 40 % (balanced in Ar) corresponds to CO_2 partial pressure of 5066, 22780, 40530 Pa, respectively. Reaction orders, calculated by applying power law model or shrinking model for kinetic reactions of dry reforming, varies from 0.27-0.35. It should be noticed that the reactivity of humin depend on the conversion levels. The low value of reaction order is another proof for the inert nature of

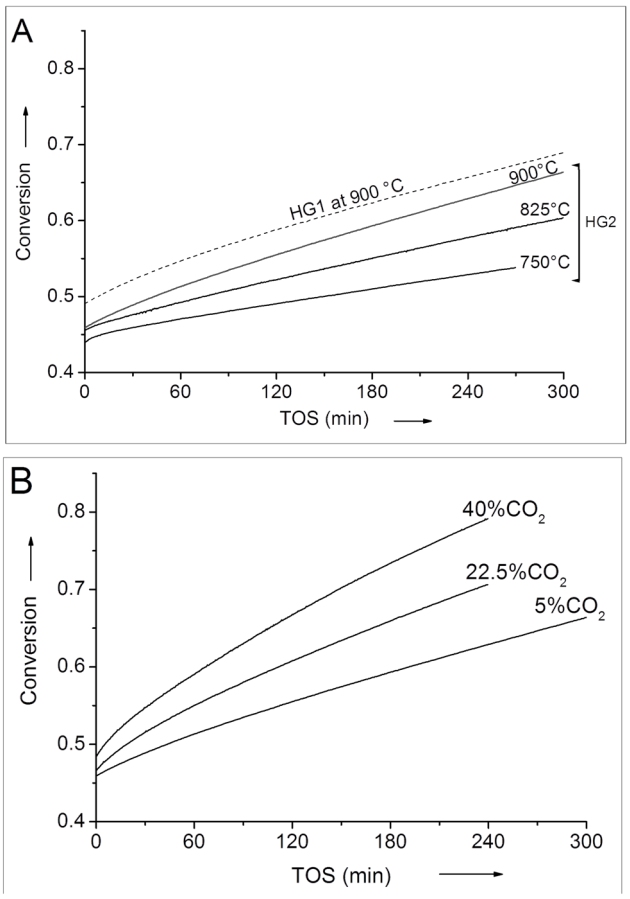

Figure 12. Non-catalytic dry reforming of humin (HG2): A – influence of temperature (isothermal temperature at 750-900°C, $(CO_2 + Ar)_{reactive}/Ar_{protective}$ = (5 + 75)/20 ml/min); B – influence of CO_2 partial pressure - reaction order (T = 900 °C, CO_2 = 5, 22.5 or 40 ml/min balanced in Ar). The initial conversion values correspond to weight loss in preheating step (ramp = 10 °C/min)

humin residue.

The dry reforming rate of humin is much lower compared to the steam reforming (at 900 °C, 300 minute TOS , ~ 98 % conversion was achieved in 1.75 vol.% steam/Ar compared with ~ 65 % conversion in 5 vol.% CO_2/Ar)[21]. This is due to lower oxidative reactivity of CO_2 compared with H_2O. Therefore, use of catalyst is essential to improve the dry reforming rate of humin.

3.5 Catalytic dry reforming of humin

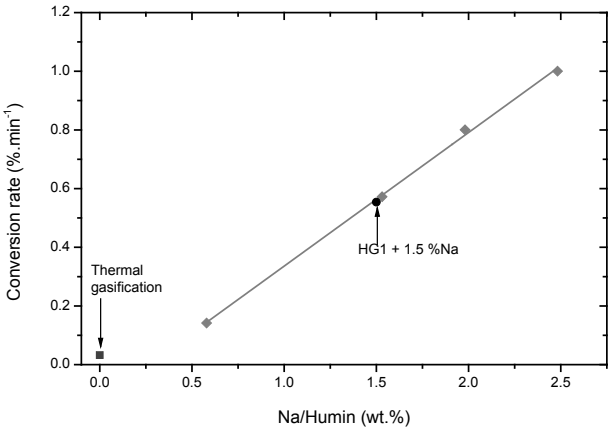

Figure 13. Influence of sodium loading on conversion rate of HG2 (diamond symbol). Round and square symbol is conversion rate of HG1 ball-milled with 1.5 wt.% Na and HG1 without catalyst, respectively. Condition: T = 700 °C, reactive gas: $(CO_2 + Ar)_{reactive}/Ar_{protective}$ = (5 + 75)/20 ml/min

We showed earlier that for steam reforming of humin, the highest activity was achieved with using Na_2CO_3 as catalyst[21]. Thus, the influence of Na_2CO_3 loading to the dry reforming rate is of interest. **Figure 13** shows the influence of sodium loading on the conversion rate. To investigate the intrinsic reactivity of humin, HG2 (*viz.* humin without entrapped sugar derivatives) is used for these experiments to avoid the influence of these impurity. It can be seen from **Figure 13** that compared with thermal reforming under the same conditions, the conversion rate is improved substantially. In the range from 0.5 to 2.5 wt.%, the conversion rate is proportional to the sodium loading. The slope derived from the linear fitting is ~ 0.45 which means ~ 0.45 wt.%. humin can be converted per minute with 1 wt.% Na loading increment. Further, the conversion rate of pristine humin (HG1) ball-milled with Na_2CO_3 also falls in the same curve (one experimental point). This implied that the reactivity of humins (HG1 and HG2) is similar and so does the influence of sodium carbonate on gasification rate of these samples. The result is in agreement with the reactivity of the samples in non-catalytic dry reforming. Hence, it is possible to conclude that the presence of entrapped sugar derivatives does not affect the overall reactivity of humin toward dry reforming reaction. For industrial application, only minimal washing of humin would be required, just enough to remove the acid catalyst (*e.g.* H_2SO_4 or HCl) used in the dehydration step.

Therefore, for industrial application, investigating the influence of gasification temperatures on the conversion, pristine humin (HG1, humin without extraction) was used and the result is illustrated in **Figure 14**. Once again, there is substantial improvement of gasification rate in the case of using Na_2CO_3. In addition, the conversion is linearly proportional to the reaction time over a wide range of conversion levels which in turn means constant conversion rate. Generally, in biomass gasification, the morphology, texture and structure of biomass residue strongly depends on the degree of conversion, thus the reaction rate can vary over the conversion range[59]. However, in this case both reaction rate (**Figure 14-B**) and the activation energy of dry reforming reaction estimated from Arrhenius plot (**Figure 14**) are almost constant in the conversion range from

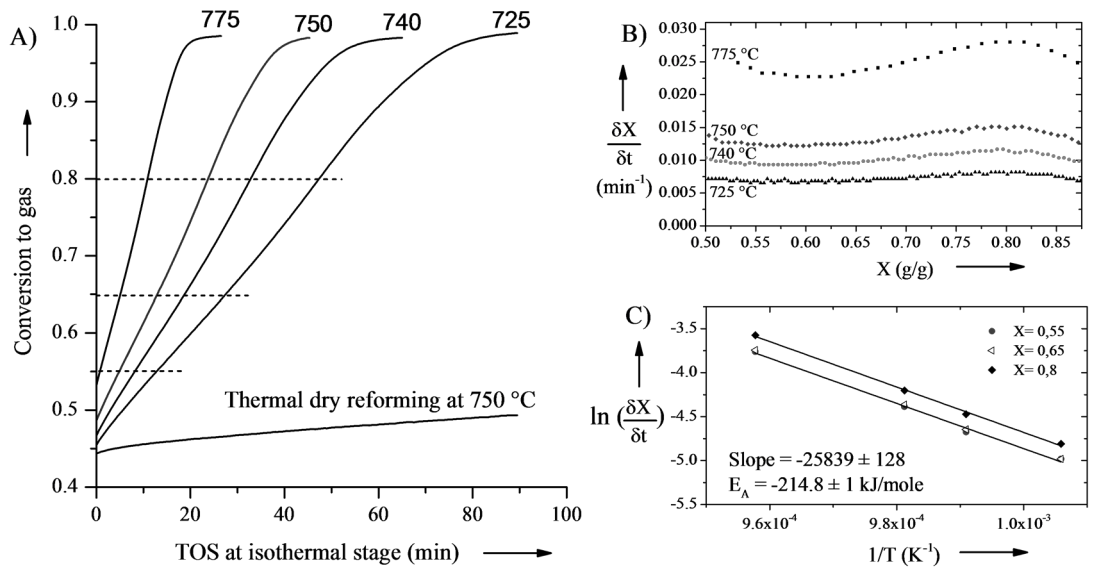

Figure 14. Isothermal conversion of HG1 ball-milled with Na_2CO_3 at various dry reforming temperatures (A), conversion rate *vs.* conversion (B) and the Arrhenius plot at conversion of 0.55 (•), 0.65 (◁) and 0.8 (♦) respectively. Heating rate 10 °C .min^{-1}; gas flowrate $(CO_2 + Ar)_{reactive}/Ar_{protective}$ = (40 + 20)/40 ml/min; P = 1 atm; Na/Humin ~ 1.5 wt.%

0.45 (initial conversion value of dry reforming stage) to ~ 0.9. A linear relationship between conversion and reaction time could also be observed when reactive gas composition changed (See **Figure S6,** supplementary information) or with variation in catalyst loading (**Figure 13**). The catalytic dry reforming of humin in presence of Na_2CO_3 proceeded evenly and resembled bulk reaction. The activation energy of 214 ± 1 kJ.mol^{-1} for dry reforming in the presence of Na_2CO_3 (calculated from Arrhenius plot, **Figure 14**) is in the same range for dry reforming of bio-derived char as summarised in the review on combustion and gasification of char by Blasi[59]. This high activation energy indirectly implies there is no mass transfer limitation during the reaction. HR-SEM image of residue obtained after heating mixture of humin with Na_2CO_3 to 700 °C did not show the hollow structure of humin as seen in non-catalytic dry reforming due to enhanced gasification rate at the external surface (the shell).

4. Conclusions

Humin formation is one of the major problems in conversion of carbohydrates to value added platform chemicals (*e.g.*, HMF, LA, and FF). Despite the high humin yields often reported, understanding of the pathways of its formation, chemical structure as well as its application in bio-refinery scheme is still limited. Structural analysis of humin and humin fractions were done in this study in addition to investigation of the influence of thermal treatment on humin which can help understand the characteristics of humin. Although pristine humin has complex furan-rich structure with multiple oxygen functional groups, heating humin at elevated temperature (to reach reforming temperature) leads to de-volatilisation and aromatisation/ graphitisation. The volatile organic components released during heating consisting of mainly phenols, aromatic hydrocarbon, furans can be used as a source of potential chemicals or further reformed to syngas/H_2 in a second stage thereby converting the whole humin feedstock. Only graphitic type carbon structure is left prior the gasification. Its inert nature causes the non-catalytic dry reforming very difficult at mild gasification conditions (below 1000 °C). The use of cheap catalyst developed, Na_2CO_3, improves the reforming rate tremendously, making the process more viable. The presence of entrapped by-products from dehydration of sugar in humin framework does not affect overall reactivity of humin in dry reforming negating a purification stage before gasification. Additionally, we believe that the result on characteristics of humin upon treatment temperatures can be useful and applied for other conversion routes of humin (*e.g.*, hydro-treating) in which elevated temperatures are required.

Acknowledgements

This research has been performed within the framework of the CatchBio program. The authors gratefully acknowledge the support of the Smart Mix Program of the Netherlands Ministry of Economic Affairs, Agriculture and Innovation and the Netherlands Ministry of Education, Culture and Science, project number 053.70.113. The authors are also grateful to C. P. Reed for ESI-MS, K. R. Nidadavolu for ATR-IR measurement, T.S. Nguyen for pyrolysis/GC-MS analysis and Ing. B. Geerdink for technical support. Prof. Erik Heeres, Henk van de Bovenkamp and Yuehu Wang (University of Groningen) were acknowledged for assisting in humin synthesis.

Notes and references

1. L. H. Zhang, C. B. Xu and P. Champagne, *Energy Conversion and Management*, 2010, **51**, 969-982.
2. C. Delgado-Andrade, I. Seiquer, M. P. Navarro and F. J. Morales, *Mol. Nutr. Food Res.*, 2007, **51**, 341.
3. A. J. Ragauskas, C. K. Williams, B. H. Davison, G. Britovsek, J. Cairney, C. A. Eckert, W. J. Frederick, Jr., J. P. Hallett, D. J. Leak, C. L. Liotta, J. R. Mielenz, R. Murphy, R. Templer and T. Tschaplinski, *Science*, 2006, **311**, 484-489.
4. Y. Sun and J. Cheng, *Bioresource technology*, 2002, **83**, 1-11.
5. S. G. Wettstein, D. M. Alonso, E. I. Gürbüz and J. A. Dumesic, *Current Opinion in Chemical Engineering*, 2012, **1**, 218-224.
6. B. Kamm and M. Kamm, *Applied microbiology and biotechnology*, 2004, **64**, 137-145.
7. T. Werpy and G. Petersen, *Top Value Added Chemicals from Biomass: Volume 1—Results of Screening for Potential Candidates from Sugars and Synthesis Gas*, National Renewable Energy Laboratory, 2004.
8. J. J. Bozell and G. R. Petersen, *Green Chemistry*, 2010, **12**, 539.
9. B. F. M. Kuster and H. S. van der Baan, *Carbohydrate research*, 1977, **54**, 165-176.
10. B. F. M. Kuster, *Carbohydrate research*, 1977, **54**, 177-183.
11. B. F. M. Kuster and H. M. G. Temmink, *Carbohydrate research*, 1977, **54**, 185-191.
12. M. J. Antal, W. S. L. Mok and G. N. Richards, *Carbohydrate research*, 1990, **199**, 91-109.
13. G. W. Huber, J. N. Chheda, C. J. Barrett and J. A. Dumesic, *Science*, 2005, **308**, 1446-1450.
14. G. W. Huber and J. A. Dumesic, *Catalysis Today*, 2006, **111**, 119-132.
15. D. M. Alonso, S. G. Wettstein, J. Q. Bond, T. W. Root and J. A. Dumesic, *ChemSusChem*, 2011, **4**, 1078-1081.
16. S. W. Fitzpatrick, *United States Patent*, 1997, **US5608105**.
17. B. F. M. Kuster and L. M. Tebbens, *Carbohydrate Research*, 1977, **54**, 158-164.
18. B. Girisuta, L. P. B. M. Janssen and H. J. Heeres, *Green Chemistry*, 2006, **8**, 701.
19. N. Shi, Q. Y. Liu, Q. Zhang, T. J. Wang and L. L. Ma, *Green Chemistry*, 2013, **15**, 1967-1974.
20. D. M. Alonso, J. Q. Bond and J. A. Dumesic, *Green Chemistry*, 2010, **12**, 1493-1513.
21. T. M. C. Hoang, L. Lefferts and K. Seshan, *ChemSusChem*, 2013, **6**, 1651-1658.
22. D. W. Mckee, C. L. Spiro, P. G. Kosky and E. J. Lamby, *Fuel*, 1983, **62**, 217-220.
23. K. Lourvanij and G. L. Rorrer, *Appl Catal a-Gen*, 1994, **109**, 147-165.
24. A. Dias, M. Pillinger and A. Valente, *Journal of Catalysis*, 2005, **229**, 414-423.
25. A. S. Dias, S. Lima, P. Brandão, M. Pillinger, J. Rocha and A. A. Valente, *Catalysis Letters*, 2006, **108**, 179-186.
26. A. S. Dias, S. Lima, M. Pillinger and A. A. Valente, *Carbohydrate research*, 2006, **341**, 2946-2953.
27. A. S. Dias, M. Pillinger and A. A. Valente, *Microporous and Mesoporous Materials*, 2006, **94**, 214-225.

28. B. Girisuta, L. P. B. M. Janssen and H. J. Heeres, *Chemical Engineering Research and Design*, 2006, **84**, 339-349.
29. B. Girisuta, L. P. B. M. Janssen and H. J. Heeres, *Industrial & Engineering Chemistry Research*, 2007, **46**, 1696-1708.
30. A. Chuntanapum and Y. Matsumura, *Industrial & Engineering Chemistry Research*, 2009, **48**, 9837-9846.
31. H. Heeres, R. Handana, D. Chunai, C. Borromeus Rasrendra, B. Girisuta and H. Jan Heeres, *Green Chemistry*, 2009, **11**, 1247.
32. M. Chidambaram and A. T. Bell, *Green Chemistry*, 2010, **12**, 1253-1262.
33. T. S. Hansen, J. Mielby and A. Riisager, *Green Chemistry*, 2011, **13**, 109-114.
34. X. Hu and C. Z. Li, *Green Chemistry*, 2011, **13**, 1676-1679.
35. X. Hu, C. Lievens, A. Larcher and C. Z. Li, *Bioresource technology*, 2011, **102**, 10104-10113.
36. R. Weingarten, G. A. Tompsett, W. C. Conner and G. W. Huber, *Journal of Catalysis*, 2011, **279**, 174-182.
37. W. Yang and A. Sen, *ChemSusChem*, 2011, **4**, 349-352.
38. K. Beckerle and J. Okuda, *J Mol Catal a-Chem*, 2012, **356**, 158-164.
39. X. Hu, C. Lievens and C. Z. Li, *ChemSusChem*, 2012, **5**, 1427-1434.
40. R. Weingarten, J. Cho, R. Xing, W. C. Conner, Jr. and G. W. Huber, *ChemSusChem*, 2012, **5**, 1280-1290.
41. R. Weingarten, W. C. Conner and G. W. Huber, *Energy & Environmental Science*, 2012, **5**, 7559-7574.
42. Y. Yang, C. Hu and M. M. Abu-Omar, *Bioresource technology*, 2012, **116**, 190-194.
43. J. M. R. Gallo, D. M. Alonso, M. A. Mellmer and J. A. Dumesic, *Green Chemistry*, 2013, **15**, 85-90.
44. X. Hu, L. Wu, Y. Wang, Y. Song, D. Mourant, R. Gunawan, M. Gholizadeh and C. Z. Li, *Bioresource technology*, 2013, **133**, 469-474.
45. V. V. Ordomsky, V. L. Sushkevich, J. C. Schouten, J. van der Schaaf and T. A. Nijhuis, *Journal of Catalysis*, 2013, **300**, 37-46.
46. T. S. Nguyen, M. Zabeti, L. Lefferts, G. Brem and K. Seshan, *Biomass and Bioenergy*, 2013, **48**, 100-110.
47. I. van Zandvoort, Y. Wang, C. B. Rasrendra, E. R. van Eck, P. C. Bruijnincx, H. J. Heeres and B. M. Weckhuysen, *ChemSusChem*, 2013.
48. N. Baccile, G. Laurent, F. Babonneau, F. Fayon, M.-M. Titirici and M. Antonietti, *The Journal of Physical Chemistry C*, 2009, **113**, 9644-9654.
49. C. Yao, Y. Shin, L. Q. Wang, C. F. Windisch, W. D. Samuels, B. W. Arey, C. Wang, W. M. Risen and G. J. Exarhos, *Journal of Physical Chemistry C*, 2007, **111**, 15141-15145.
50. Y. M. Xiaodong Xu, Jonny Stenberg, and Michael Jerry Antal, Jr.*, *Industrial-and-Engineering-Chemistry-Research*, 1996, **35**, 9.
51. G. Almendros, J. Sanz and L. Sobrados, *The Science of the Total Environment,*, 1989, **81-82**, 91-98.
52. C. Falco, N. Baccile and M.-M. Titirici, *Green Chemistry*, 2011, **13**, 3273.
53. R. K. Sharma, J. B. Wooten, V. L. Baliga and M. R. Hajaligol, *Fuel*, 2001, **80**, 1825-1836.
54. C. Falco, F. Perez Caballero, F. Babonneau, C. Gervais, G. Laurent, M. M. Titirici and N. Baccile, *Langmuir : the ACS journal of surfaces and colloids*, 2011, **27**, 14460-14471.
55. A. C. Ferrari and J. Robertson, *Philosophical transactions. Series A, Mathematical, physical, and engineering sciences*, 2004, **362**, 2477-2512.
56. M. Sevilla and A. B. Fuertes, *Carbon*, 2009, **47**, 2281-2289.
57. X. J. Li, J. Hayashi and C. Z. Li, *Fuel*, 2006, **85**, 1700-1707.
58. P. Ollero, A. Serrera, R. Arjona and S. Alcantarilla, *Biomass Bioenerg*, 2003, **24**, 151-161.
59. C. Di Blasi, *Progress in Energy and Combustion Science*, 2009, **35**, 121-140.